MASTER

UCID- 18086

Lawrence Livermore Laboratory

THICK-TARGET NEUTRON AND γ-RAY YIELDS INDUCED BY MEDIUM-ENERGY PROTON AND DEUTERON BOMBARDMENTS

J. A. Becker
R. E. Howe
K. W. Crase
E. Farley

March 7, 1979

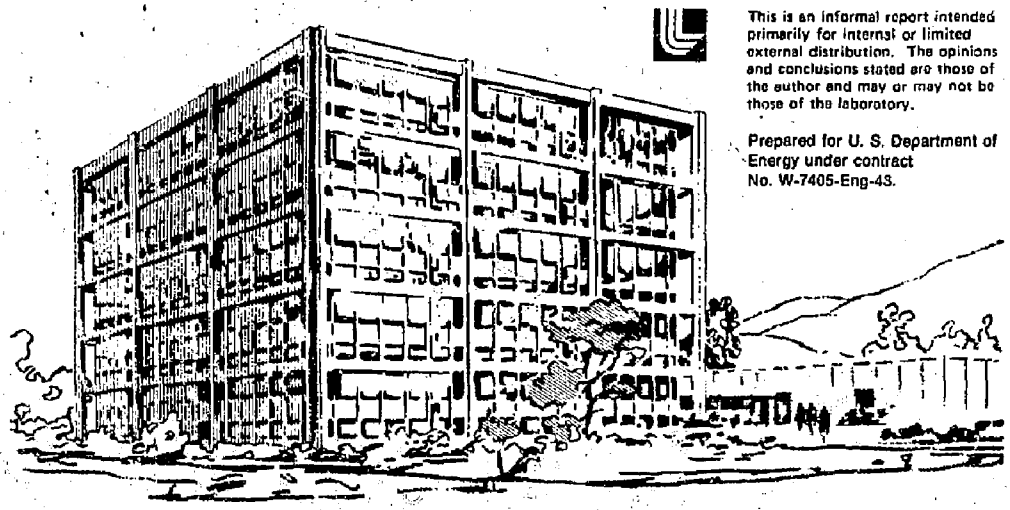

THICK-TARGET NEUTRON AND γ-RAY YIELDS INDUCED BY MEDIUM-ENERGY PROTON AND DEUTERON BOMBARDMENTS†

J. A. Becker, R. E. Howe, K. W. Crase, and E. Farley

Lawrence Livermore Laboratory
University of California
Livermore, California 94550

ABSTRACT

Stopping samples of Lucite, Al, Fe, and ^{238}U (Fe, and ^{238}U) were irradiated with 330 MeV deuterons (260 MeV protons). For each target, neutron energy spectra and prompt γ-ray yields were measured using the time-of-flight technique. The detector was a right cylindrical volume of deuterated benzene, 12.5-cm diameter x 7.5-cm long, located at 110° to the incident beam direction. The neutron yield and the prompt γ-ray yield were found to depend upon the atomic number of the target and upon the incident projectile. The measured shape of the neutron energy spectrum was not strongly dependent on either the incident projectile or the target atomic number. A lower limit for absolute neutron yields was also obtained.

†This work was sponsored by the Ballistic Missile Defense Advanced Technology center, Huntsville, Alabama, under Military Interdepartmental Purchase Request No. W-31 RPD-93-Z-169.
The contract monitor was Dr. Larry Havard.

I. INTRODUCTION

Information on the yield and energy distribution of neutrons and of photons produced in spallation reactions is limited. This is particularly true for photons. Such information has obvious practical uses as, for example, in accelerator shielding design; at the same time, model predictions of the interaction process can be compared with experimental results. An experiment to gain some information on these points is described below. Targets drawn from a wide range of the periodic table were bombarded with 260 MeV protons and with 330 MeV deuterons. Yields of neutrons and of prompt γ-radiation were obtained, together with neutron energy spectra.

II. EXPERIMENT

Targets thick enough to stop the incident beam were bombarded with either 330 MeV deuterons or 260 MeV protons accelerated by the LBL Bevatron. Table 1 contains the target details. Beam currents were on the order of 1-4 x 10^7 particles per pulse. The beam pulse macrostructure was nominally 0.5 sec in duration, with a 4 second period; the microstructure had a nominal frequency of 1.5 MHz, and the beam packets were roughly 40 nsec wide. The beam packets were also modulated, so that the instantaneous current might well reach $\sim 10^{10}$-10^{11} particles/sec. Reaction neutrons and γ-rays were detected in a liquid scintillator located with its front face 250 cm from the reaction site. The scintillator was primarily deuterated benzene, contained in a right cylinder 12.5-cm diameter by 7.5-cm long. The pulse-shape discrimination technique was used to distinguish between neutrons and γ-rays. Neutron energy was measured using the time-of-flight technique. One

channel of time information was derived from the accelerator rf, thus presenting a signal synchronous with the time of arrival of the beam packet at the target; a pulse derived from the detector output provided the other piece of time information. The time-of-flight system was calibrated using known delays. The detector was housed in a lead and boric-acid cave: no less than 10 cm of Pb surrounded the detector, and the lead in turn was encased in no less than 7.5-cm of boric acid. A 10x10-cm NaI(Tℓ) detector was also in the cave, placed alongside the liquid scintillator and separated from it by a 5-cm thickness of Pb. The threshold of the neutron spectrometer was on the order of 150-keV electron energy, or about 0.9-MeV neutron energy. A Pb sheet, 1.2-cm thick, was placed between the target and detector to absorb low energy γ-radiation. The detector efficiency was calibrated in the experimental geometry using a ^{252}Cf source located at the reaction site. The source was contained within an ionization chamber; in order to obtain a time-of-flight spectrum, shaped pulses from the ionization chamber were used instead of pulses derived from the Bevatron rf signal.

Data were obtained for approximately 15 minutes of bombardment time for each target. Beam currents were monitored in a Bevatron supplied ionization chamber placed upstream in the beam path. Beam profile at the target was monitored using a Bevatron supplied multi-wire proportional counters. The beam spot at the target was 8-cm (FWHM) for the deuteron runs. For the proton runs, the beam energy E_p = 260 MeV was obtained by the use of a 13.0-cm thick Al degrader placed in the beam path 254 cm upstream of the target; the beam spot on target was estimated to be 11 cm in diameter (FWHM).

III. RESULTS

The pulse-shape discriminator associates every event above threshold in the liquid scintillator with either a neutron or γ-ray incident upon the detector. Thus, using halves of a multichannel analyzer and the identification signal, neutron and γ-ray spectra were obtained for each target listed in Table 1 simultaneously. The neutron time-of-flight spectra are shown in Figs. 1-7, while the corresponding γ-ray time distributions are illustrated in Figs. 8-14.

The neutron time-of-flight spectra (Figs. 1-7) are characterized by an evaporation type distribution with a maximum near E_n=3-4 MeV, together with a peak due to misidentified prompt γ-rays (near channel 322 in Fig. 2) and identified on the upper abcissa scale as "γ". At the low energy end of the spectrum, a contribution from room scattered neutrons is evident as well as another contribution from misidentified γ-radiation. This later contribution is time independent and originates in delayed γ-ray activity. When these spectra are examined it must be remembered that due to the beam microstructure, the time resolution is ∿ 40 nsec (FWHM). Thus, events in the spectrum due to high energy neutrons and prompt γ-rays overlap. In Fig. 1-7, the upper abcissa scale labels the neutron energy, deduced from the time calibration (1.41 nsec/channel) and the length of the flight path. Gamma-ray time distribution spectra are shown in Figs. 8-14. The γ-ray spectra exhibit a "prompt" γ-ray peak superimposed upon a long term time independent background, representing for the most part beam induced delayed activity. This is illustrated in Fig. 9 spectrum associated with deuteron bombardment of Al. The full width half maximum (FWHM) of the time distribution is found from this data to be 42 nsec (30 channels).

The neutron yield was extracted from each spectrum using a simple procedure described below: The spectrum illustrated in Fig. 2 will serve as an example. The yield of neutrons plus background was obtained by integration over the energy region corresponding to channels 193 to 353. The background was estimated from the low energy region of the spectrum, channels 10-54. Assuming that the background is proportional to the time interval, the net neutron yield was obtained by subtraction. The high energy integration limit was chosen to include the contribution to the yield from high energy neutrons and therefore includes a contribution of misidentified prompt γ-ray radiation. Evidently this procedure will overestimate the yield for the lighter targets where the misidentified γ-ray peak is in evidence; the error was not significant enough to justify detailed fitting at this point. Prompt γ-ray yields were obtained in a similar fashion. Table II lists 1) the integrated counts of both neutrons and prompt γ-rays obtained in this fashion, 2) these yields normalized with negligible error to the ionization chamber current, and 3) the ratio of the two yields.

A detailed examination of the shape of the neutron time-of-flight spectra reveals some interesting features. For target ^{238}U, the spectral shape is independent of the bombarding particle type (p or d). The same statement applies to the spectra obtained with the Fe target, although with less certainty. This is because the neutron time-of-flight spectrum associated with the proton bombardment of Fe has poor statistics. Also, it was obtained with intermittent beam conditions and so the γ-ray time independent background is high. It is difficult to ascertain from these data whether or not the neutron spectra

changes in any significant way with target mass number.

When the spectrum resulting from deuteron bombardment of Al (Fig. 2) is compared with the spectrum resulting from deuteron bombardment of ^{238}U (Fig. 4), the only shape difference is the pronounced peak in the Al spectrum due to misidentified γ-rays. When the spectrum resulting from the bombardment of an Fe target (Fig. 3) is compared with that resulting from bombardment of ^{238}U, there is a suggestion of a slightly different slope for $E_n > 8$ MeV such that the spectrum associated with the Fe target is slightly harder than that due to the ^{238}U target. However this difference becomes insignificant when a small amount of misidentified γ-radiation is mixed in and when statistics are considered. The same statement may be made when the spectrum produced by the lucite target (Fig. 1) is compared with the spectrum associated with the ^{238}U target. These data exhibit no evidence of a change in the neutron energy spectrum as a function of target atomic number. The yield of neutrons is sensitive to both the target atomic number and the type of bomarding particle (p or d). During data collection, the incident beam was monitored through the charge collected in an ionization chamber located in the beam line. The ionization chamber output counter was calibrated in a separate procedure, and in terms of the entries in Table II, Column 4, one ionization chamber count represents either 1.0×10^6 protons or 5.3×10^5 deuterons, appropriately.

Columns 7 and 8 of Table II present the neutron and γ-ray counts per incident particle. It is clear that both the neutron and γ-ray yield increase with increasing target atomic number, particularly the neutron yield. In Table III, the neutron and γ-yields and the ratio of the two are compared to the corresponding entries when ^{238}U is the target. The absolute calibration must be viewed with some caution, since it represents a best choice from somewhat conflicting results. An estimate of the calibration error may be deduced by considering the relative neutron yields resulting from bombardment of the same target by deuterons and protons, and measuring the relative number of incident particles with the ionization chamber. Considering (i) at the appropriate energies $(dE/dx)_d = 1.5(dE/dx)_p$, and (ii) there is a 70% fluence loss at the target for proton beams due to the Al energy degrader, the ratio of neutron yield produced by deuteron bombardment to neutron yield produced by proton bombardment is 1.4 and 1.6 for the ^{238}U and Fe targets, respectively. The corresponding quantities from column 7 of Table II are 5.7 and 6.8.

An estimate of the absolute cross section may be obtained if the calibration of the ionization chamber which monitors the incident beam is known and if the counter efficiency as a function of neutron energy is known. The efficiency of the counter may be measured by counting a ^{252}Cf source placed at the sample site for a known time interval. Figs. 15 and 16 illustrate the neutron and γ-ray time-of-flight spectra, respectively, for the ^{252}Cf source. The source was counted in the experimental geometry with the same electronic arrangement. For the ^{252}Cf fission neutron spectrum, it was found that the detector had a counting efficiency per fission of $(6.61 \pm 0.66) \times 10^{-3}$%. An arbitrary error of 10% is assigned to the source strength. The absolute calibration of the ionization chamber is given above. Assuming that the neutron emission spectrum is

similar for spallation reactions and fission, an estimate of the absolute cross section may be obtained using this efficiency. However, it is clear that the ^{252}Cf spectral shape is quite different from the spectral shape measured with e.g., a ^{238}U target: the spallation spectrum exhibits a great many more high energy neutrons than the ^{252}Cf spontaneous fission spectrum. Thus this procedure of obtaining an absolute measurement is only a rough one (suitable however for field use).

Very little information was obtained on the prompt γ-ray pulse height distribution with the experimental arrangement described, because of pulse-pile up during the beam pulse. A visual inspection of the pulse height suggested that the heavier targets had some γ-rays with energy greater than 2 MeV associated with them. Another source of evidence for differences in the γ-ray spectra is contained in the neutron time-of-flight spectra. Because of the nature of the pulse-shape discrimination processes, γ-ray pulses corresponding to low energy γ-ray events may be mistakenly identified as neutron events, and thus appear in the neutron spectra. Prompt events appear in the neutron time-of-flight spectrum corresponding to the velocity c. Examination of the neutron time-of-flight spectra indicates that the ratio of low-energy γ-rays to neutrons varies from target to target, suggesting a change in the γ-ray pulse-height distribution with target.

Table 1. Target Details

Target	Lucite	Al	Fe	^{238}U
Thickness (cm)	32.70	17.78	7.62	5.08

Table 2. Net neutron (n) and prompt γ-ray (γ) yields. Statistical errors are estimated to be 10% in yield, and 14% in the ratio of neutron yield to γ-ray yield.

Run #	Target	Beam	Ionization	Net Yield		$\frac{\text{Yield} \times 10^6}{\text{Incident particle}}$		Ratio
				n	γ	n	γ	n/γ
3	Al	d	1163	14052	8119	22.8	13.1	1.73
4	^{238}U	d	619	29524	7222	89.8	21.9	4.08
5	Lucite	d	685	4168	2561	11.4	7.0	1.62
6	Blank	d	717	886	479	2.3	1.3	1.23
7	Fe	d	745	9691	6456	24.5	16.3	1.50
9	^{238}U	p	1367	21603	5098	15.8	3.7	4.23
10	Fe	p	1184	4309	3320	3.6	2.8	1.29
11	^{252}Cf	-	-	240603	238155	-	-	1.01

Table 3. Neutron yields, γ-ray yields, and their ratio for various targets normalized to the respective quantities for a ^{238}U target.

Incident Particle	Target	Relative Yield	Relative γ-ray Yield	Ratio
		Target		
d	Lucite	0.13	0.32	0.40
d	Al	0.25	0.60	0.42
d	Fe	0.27	0.74	0.37
d	^{238}U	1	1	1
p	Fe	0.23	0.75	0.30
p	^{238}U	1	1	1

FIGURE CAPTIONS

Fig. 1. Neutron time-of-flight spectrum for a lucite target bombarded with 330 MeV deuterons. The detector was located at 110°.

Fig. 2. As Fig. 1, except that the target is Al.

Fig. 3. As Fig. 1, except that the target is Fe.

Fig. 4. As Fig. 1, except that the target is ^{238}U.

Fig. 5. As Fig. 1, except that a block of Al 13.02-cm thick was placed in the beam path, 254 cm upstream of the target site.

Fig. 6. Neutron time-of-flight spectrum for a Fe target bombarded by 260 MeV protons. The detector was located at 110°.

Fig. 7. As Fig. 6, except that the target is ^{238}U.

Fig. 8. γ-ray time distribution for a lucite target bombarded with 330 MeV deuterons. The detector was located at 110°.

Fig. 9. As Fig. 9, except that the target is Al.

Fig. 10. As Fig. 9, except that the target is Fe.

Fig. 11. As Fig. 9, except that the target is ^{238}U.

Fig. 12. As Fig. 9, except that a block of Al 13.02-cm thick was placed in the beam path, 254 cm upstream of the target site.

Fig. 13. γ-ray time distribution for a Fe target bombarded by 260 MeV protons. The detector angle is located at 110°.

Fig. 14. As Fig. 14, except that the target is ^{238}U.

Fig. 15. Neutron time-of-flight spectrum taken with a ^{252}Cf source (spontaneous fission) at the target site.

Fig. 16. The γ-ray time distribution corresponding to Fig. 15.

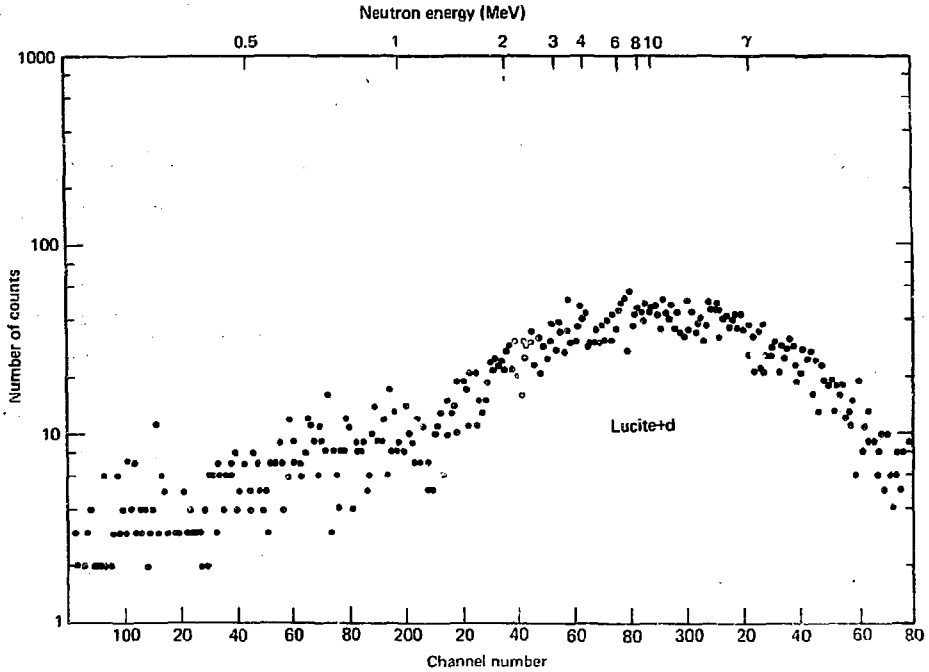

Fig. 1. Neutron time-of-flight spectrum for the lucite + d reaction.

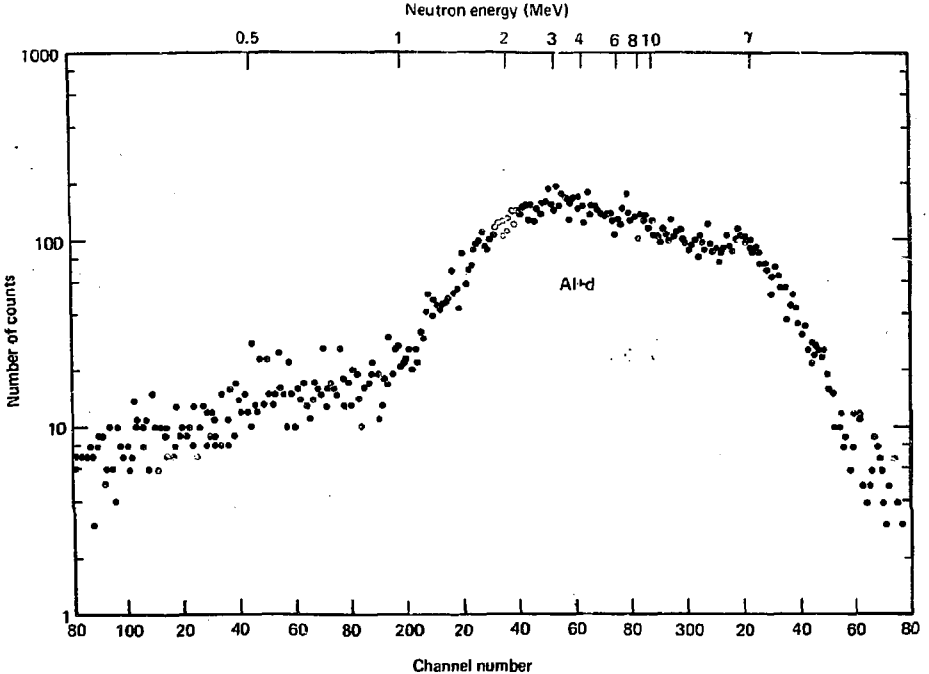

Fig. 2. Neutron time-of-flight spectrum for the Al + d reaction.

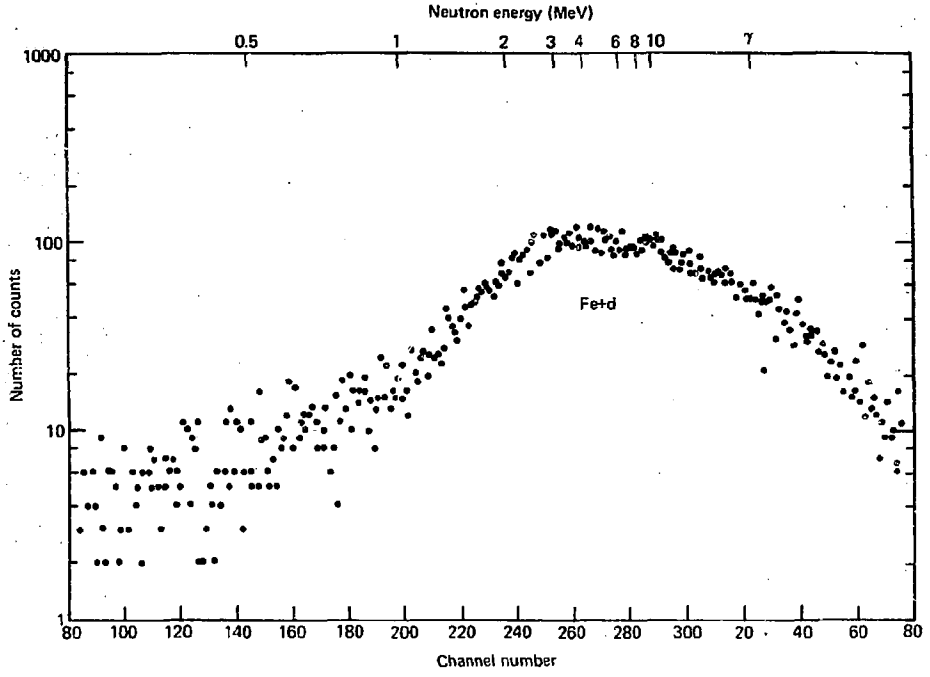

Fig. 3. Neutron time-of-flight spectrum for the Fe + d reaction.

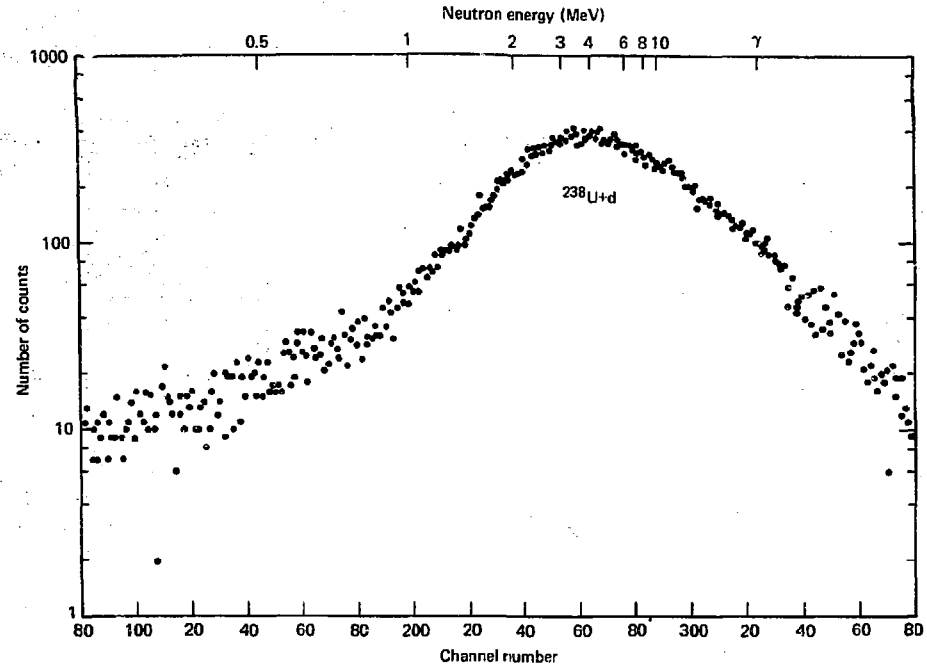

Fig. 4. Neutron time-of-flight spectrum for the ^{238}U + d reaction.

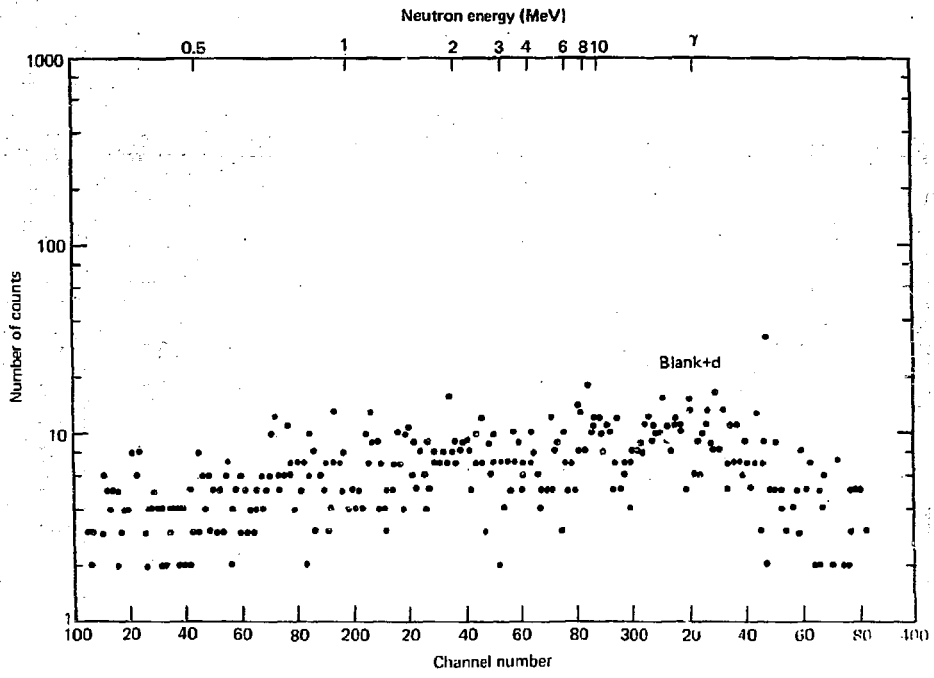

Fig. 5. Background time-of-flight spectrum.

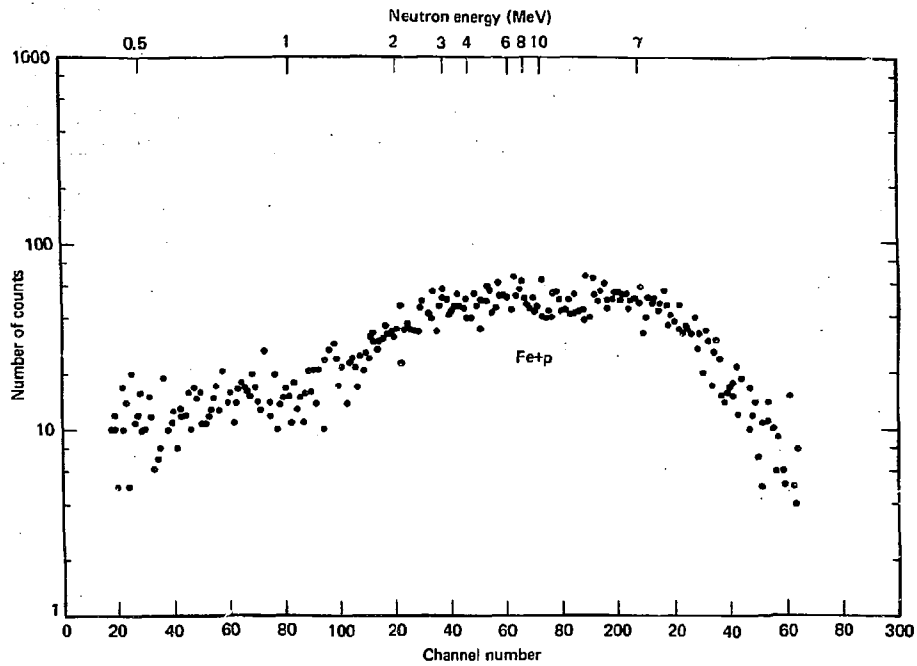

Fig. 6. Neutron time-of-flight spectrum for the Fe + p reactions.

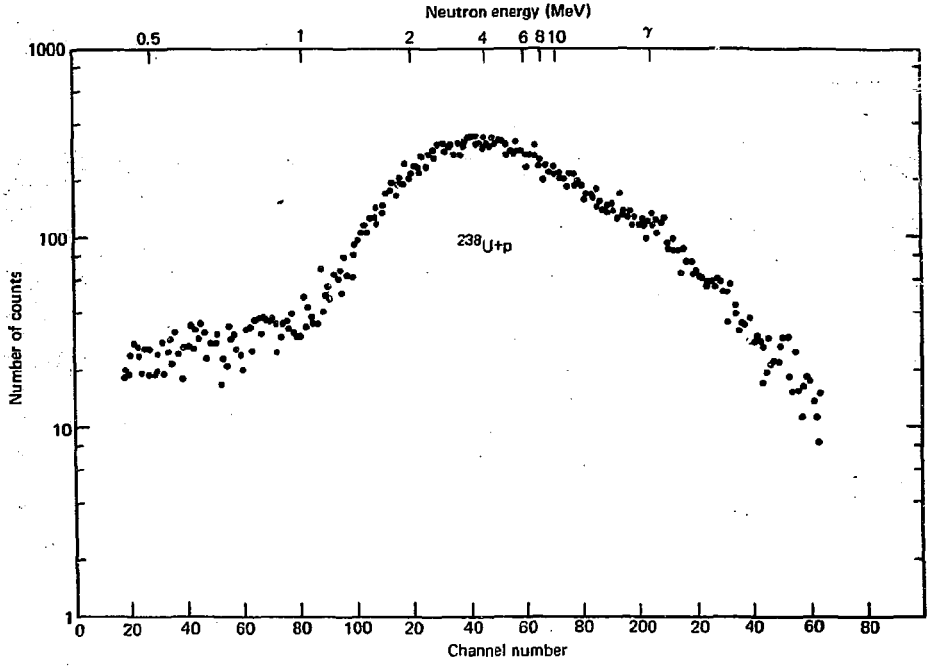

Fig. 7. Neutron time-of-flight spectrum for the ^{238}U + p reaction.

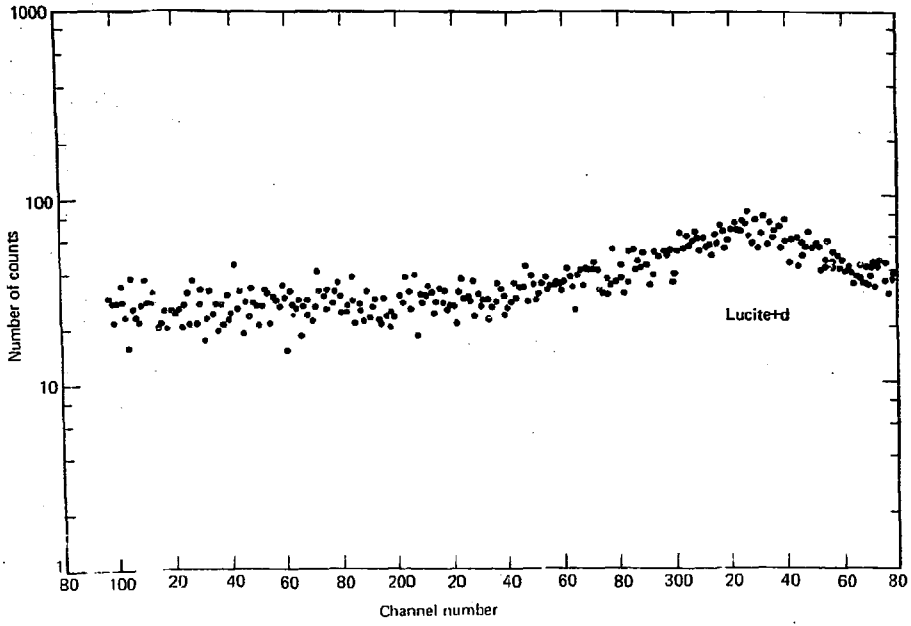

Fig. 8. The γ-ray time distribution for the lucite + d reaction.

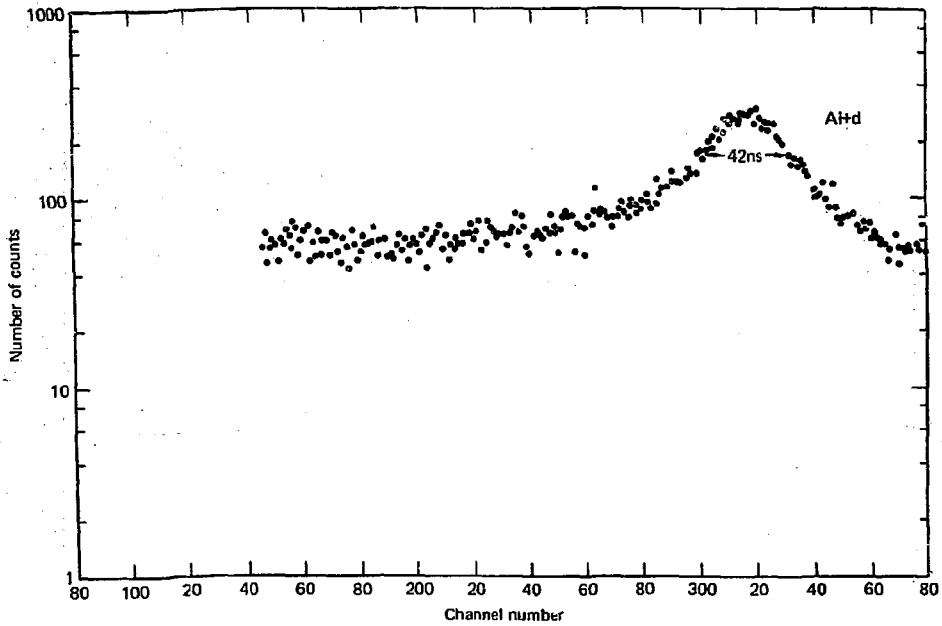

Fig. 9. The γ-ray time distribution for the Al + d reaction.

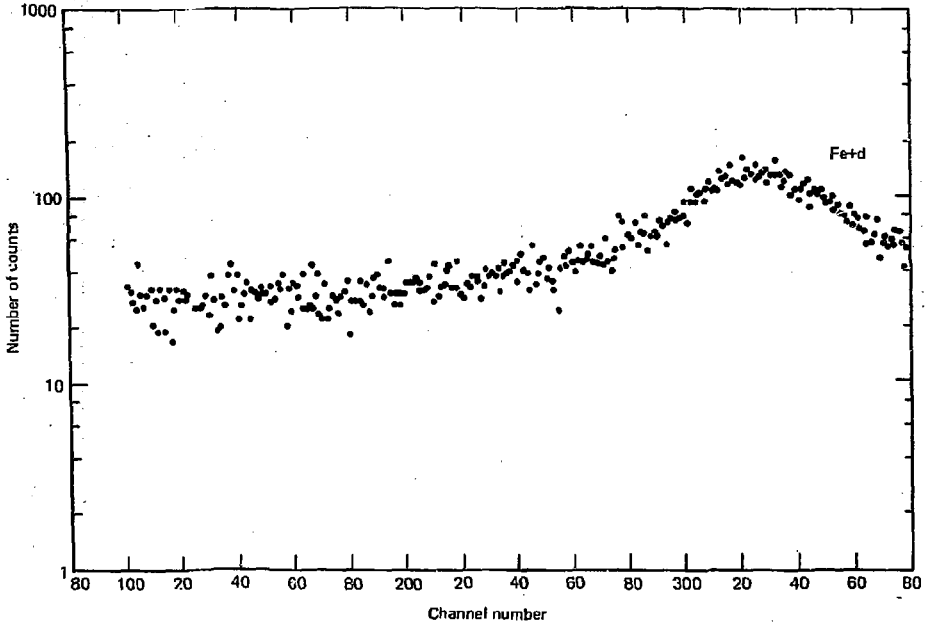

Fig. 10. The γ-ray time distribution for the Fe + d reaction.

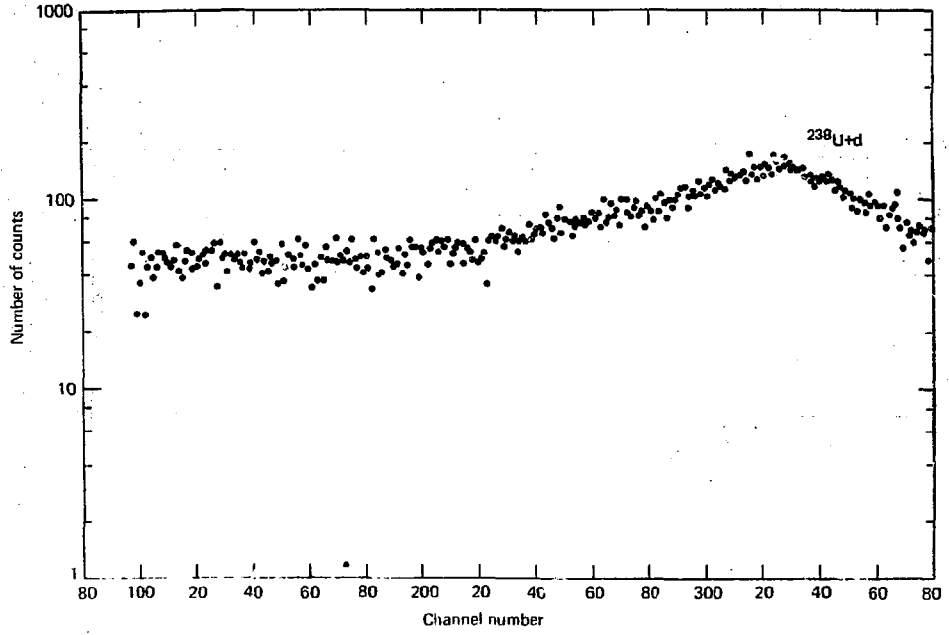

Fig. 11. The γ-ray time distribution for ^{238}U + d reaction.

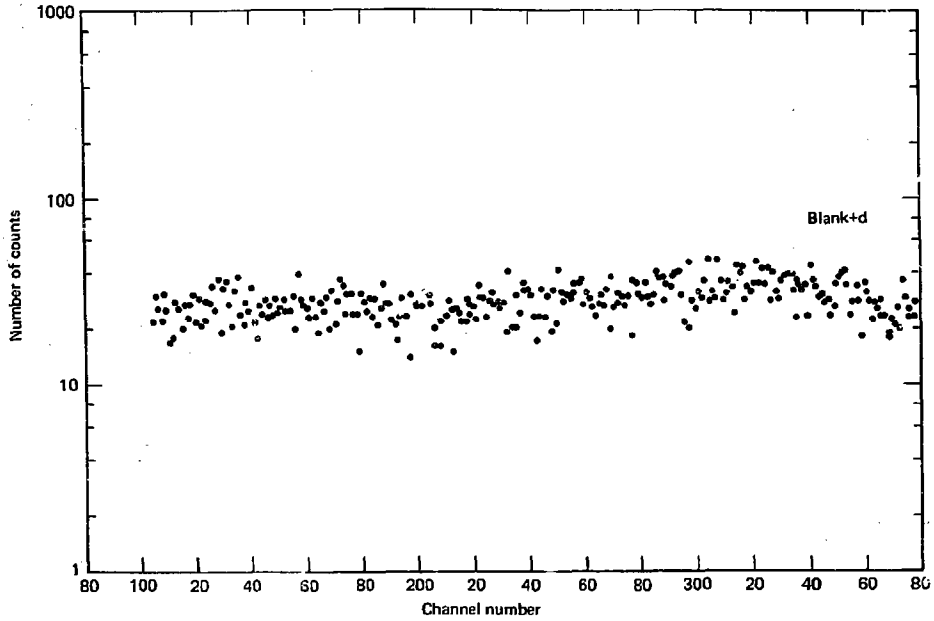

Fig. 12. Background γ-ray time distribution.

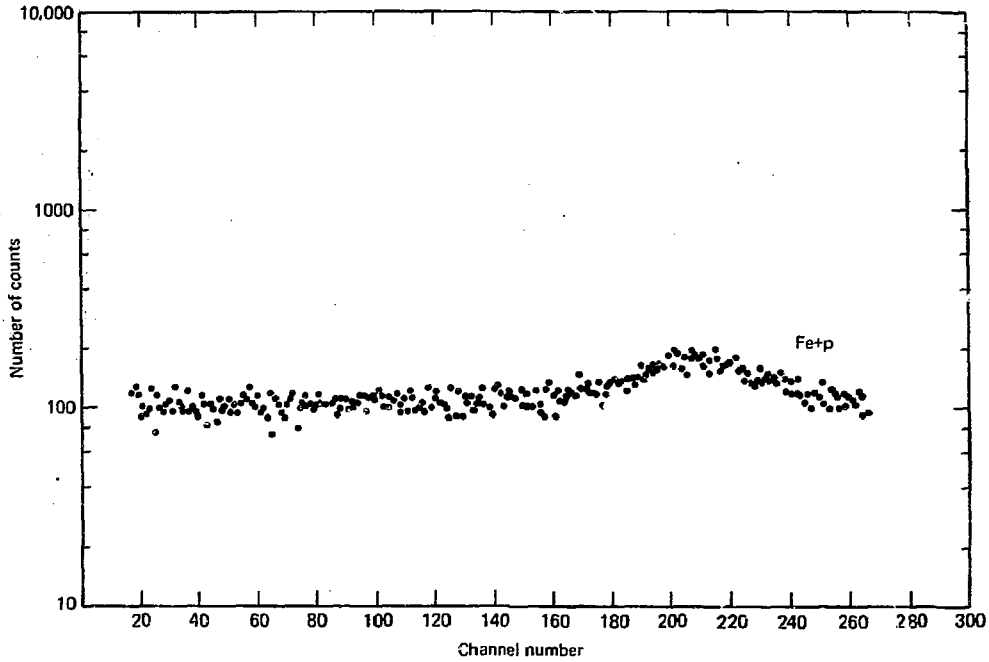

Fig. 13. The γ-ray time distribution for the Fe + p reaction.

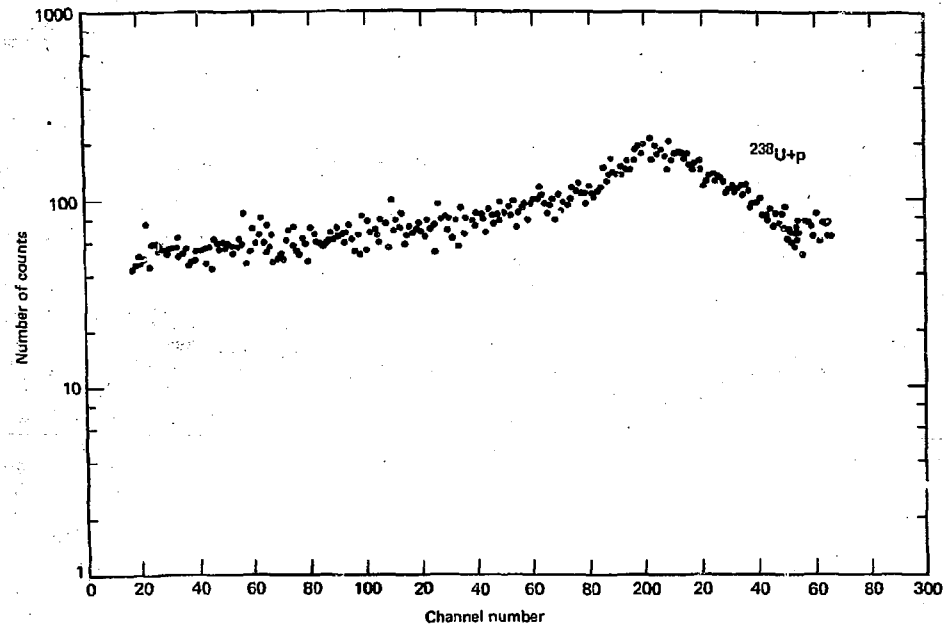

Fig. 14. The γ-ray time distribution for the ^{238}U + p reaction.

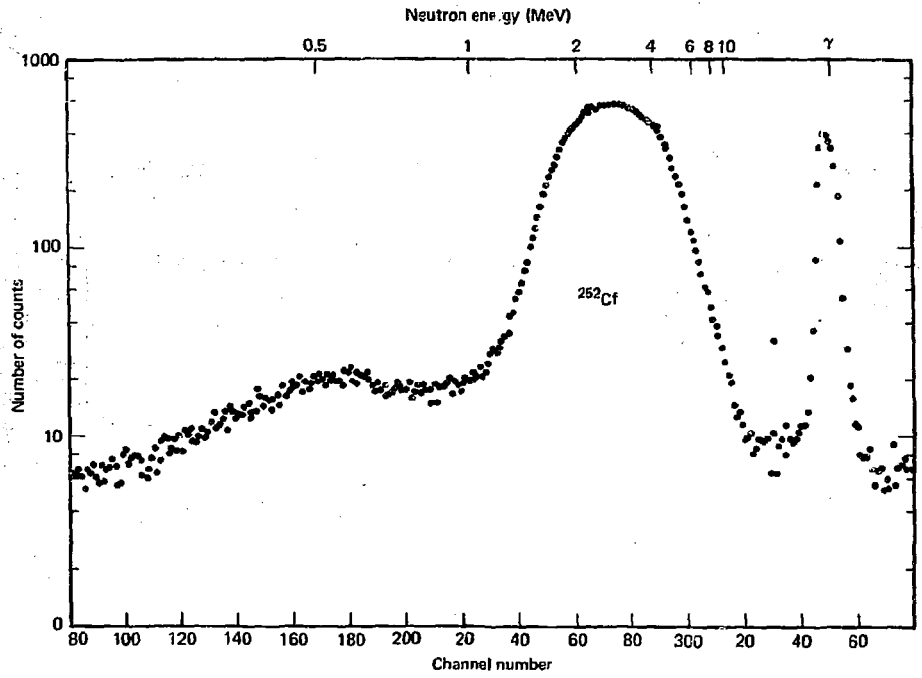

Fig. 15. Neutron time-of-flight spectrum taken with a ^{252}Cf source (spontaneous fission) at the target site.

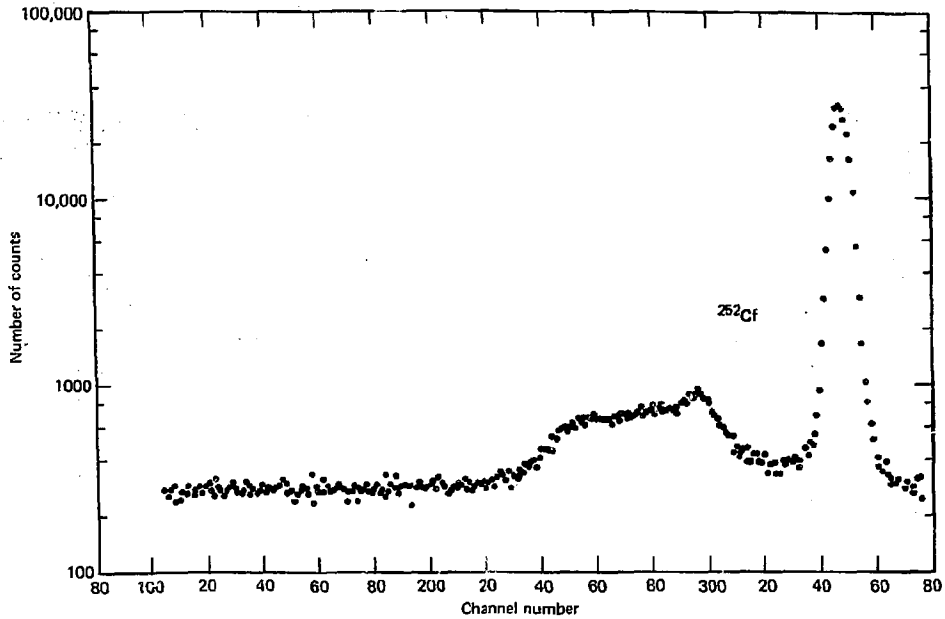

Fig. 16. The γ-ray time distribution corresponding to Fig. 15.